Particulate Modeling of Sand Slurry Flow Retardation

Modélisation par les milieux granulaires de l'effet de retard de l'écoulement des boues résiduelles

Tomac I., Gutierrez M.
Colorado School of Mines, Golden, CO, USA

ABSTRACT: The focus of this study is on the flow of dense sand slurries within a narrow channel, with a volumetric particle concentration greater than 0.1 and a ratio of channel width and particle radius less than 10. In sand slurry flow processes in narrow channels, clogging and velocity retardation often occur and are governed by the sand concentration and slurry flow rate. A numerical model developed in this study permits an improved understanding of the conditions which lead to particle clogging in sand slurry flow within narrow channels. The used numerical model couples the discrete element method (DEM) with computational fluid dynamics (CFD)to study this flow process. A user-defined contact model was developed to capture the non-linear collision of submerged particles and walls. A damping effect, formulated using the theory of lubrication associated with a thin fluid layer between particles is associated with the contact model. Lubrication is observed to enhance the formation of particle packs in the slurry flow, and decreases the kinetic energy of particle collisions.

RÉSUMÉ : Cette étude considère l'écoulement des boues de sable dense dans un canal étroit, avec une concentration en particules volumétrique supérieur à 0,1 et un rapport de largeur de canal moins de 10 rayon des particules. Dans les processus d'écoulement de boue de sable dans des chenaux étroits, le colmatage et le retard de la vitesse se produisent souvent et sont régis par la concentration en sable et le débit de la pâte. Un modèle numérique développé dans cette étude permet une meilleure compréhension des conditions qui conduisent à des particules le colmatage de l'écoulement de boue dans les chenaux étroits. Le modèle établi un couplage entre la méthode des éléments discrets et les méthodes numériques de la dynamique des fluides pour étudier ce processus. Un modèle de contact pouvant être défini par l'utilisateur a été mis au point pour représenter la collision non linéaire des particules immergées et les murs. Un effet d'amortissement, formulée en utilisant la théorie de lubrification associée à une couche mince de fluide entre les particules, est associé au modèle de contact. On observe que la lubrification d'améliore la formation des paquets de particules dans l'écoulement de suspension, et diminue l'énergie cinétique des collisions de particules.

KEYWORDS: sand, lubrication, discrete element model, computational fluid mechanics, dense phase flow

1 INTRODUCTION

Sand and other particulate material submerged in water and subjected to a fluid driven transport can be found in many geotechnical problems. For example, the stability of sand drains often fails under the increase groundwater pressure during the stabilization of excavation pit bottoms or consolidation process. Failure of dams and embankments can be caused by formation of localized fluid channels - pipes caused by seepage within the embankment body that carry out material and water (Fig. 1). Another potential application of the results from this study is the prediction of grouting effectiveness. A discrete element study is performed to better understand the sand-water slurry flow in narrow channels from a micro-mechanical point of view.

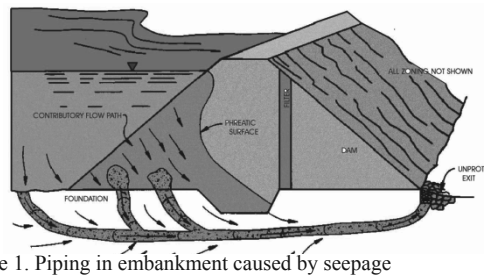

Figure 1. Piping in embankment caused by seepage

The motivation for the micro-mechanical approach comes from the multi-phase theory, which explains that at higher sand concentrations, the flow is assumed to be in category of dense phase flows, in which the particle interaction forces dominate over the fluid drag forces in the slurry behavior.

2 METHODOLOGY

Discrete element method coupled with computational fluid dynamics (CFD-DEM) in two dimensions is used with the commercialy available Particle Flow Code (PFC^{2D}) (Itasca Consulting Group, Inc. 2008a). Two-way particle fluid coupling is used to model a dense phase flow of medium coarse sand and water. Fluid motion is averaged over each fluid grid element, while particle motion is tracked individually. In the dense phase flow, particle–particle collisions dominate over the fluid drag force, because there is no sufficient time to respond to the local fluid dynamic forces before the next collision occurs. Dense flow is described with the relation (Crowe et al., 2011):

$$\frac{\tau_v}{\tau_c} = \frac{\overline{\rho}_d D v_r}{3\mu} > 1 \qquad (1)$$

where τ_v=fluid response time and τ_c=particle response time, $\overline{\rho}_d$ =bulk density of the dispersed phase (sand), D=particle diameter, v_r=relative particle velocity, μ=fluid dynamic viscosity.

In order to account for collision forces with more accuracy, a new discrete element contact model is developed for particle – particle collisions suspended in the fluid, and it is based on the elasto-hydro-dynamic theory equation that incorporates a lubrication force at particle-particle impact (Davis et al., 1986).

2.1 Continuum fluid dynamics and discrete element model

The Discrete Element Method defines a system of particles that are represented by finite spherical or disc spaces (Cundall and Strack, 1979). The motion of each particle is solved using the explicit finite difference scheme. The calculation cycle in DEM is a time-stepping algorithm that consists of repeated applications of the law of motion to each particle, the force-displacement law to each contact, and the constant updating of

wall positions. The PFC^{2D} uses simple fluid coupling scheme (Patankar, 1980) for incompressible viscous or inviscid flow on a fixed rectangular grid aligned with and superimposed on the Cartesian axes for the DEM model. The fluid flow in the PFC^{2D} uses the numerical scheme of the Navier-Stokes' equations. The effects of solids on fluid motion are introduced to the numerical scheme of the Navier–Stokes's equations in terms of porosity and coupling force averaged over each element (Bouillard et al., 1989). Fluid-solids coupling time-step is 100 times larger than individual particles collision time-step. The drag force applied by all the particles in each fluid element to the fluid is defined as:

$$\vec{f}_b = \beta \vec{U} \tag{2}$$

where $\vec{f}_b$=drag force applied to the unit volume of fluid, β=coefficient for flow, $\vec{U}$ =average relative velocity between the particles and the fluid, defined as:

$$\vec{U} = \bar{\vec{u}} - \vec{v} \tag{3}$$

where $\bar{\vec{u}}$ =average velocity of all particles in a given fluid element, $\vec{v}$ =fluid velocity. Different expressions for coefficient β are given for porosities with values higher and lower than e=0.8 (Bouillard et al. 1989):

$$\beta = \frac{(1-e)}{\bar{d}^2 e^2}(150(1-e)\mu + 1.75\rho_f \bar{d}\left|\vec{U}\right|); e < 0.8 \tag{4}$$

$$\beta = \frac{4}{3} C_d \frac{\left|\vec{U}\right|\rho_f (1-e)}{\bar{d} e^{1.7}}; e \geq 0.8 \tag{5}$$

$$C_d = \begin{cases} \dfrac{24(1+0.15\,\mathrm{Re}_p^{0.687})}{\mathrm{Re}_p}; \mathrm{Re}_p < 1000 \\ 0.44; \mathrm{Re}_p > 1000 \end{cases} \tag{6}$$

$$\mathrm{Re}_p = \frac{\left|\vec{U}\right|\rho_f e \bar{d}}{\mu} \tag{7}$$

where $\bar{d}$ =average diameter of the particles occurring in the element, C_d=turbulent drag coefficient defined in terms of particle Reynolds number Re_p, e=porosity, ρ_f=fluid density, μ=fluid dynamic viscosity. A fluid force equal and opposite acts to the particles in each fluid element. The fluid drag force applied to individual discrete particles is:

$$\vec{f}_{drag} = \frac{4}{3}\pi r^3 \frac{\vec{f}_b}{(1-e)} \tag{8}$$

where $\vec{f}_{drag}$ =fluid drag force on the particle and r=particle radius. The fluid-applied force acts at the particle center of mass, and the rotational moment is not applied to the particle. The resultant force that determines the individual particle motion is the sum of the averaged fluid drag and individual particle-particle or particle-wall collision forces and moments.

2.1.1 User defined lubrication contact model

The particle contact model in PFC2^D is built to model the elasto-hydrodynamic deformation of a solid elastic sphere that is immersed in a viscous fluid and in close motion toward another sphere or a wall. The model is based on the criteria for predicting whether two solid particles will stick or rebound subsequent to impact immersed in the fluid.

The lubrication force, $F(t)$ act as contact force when two spheres are approaching each other (Davis et al., 1986):

$$F(t) = \frac{6\pi\mu a^2 v}{x} \tag{9}$$

where μ=fluid dynamic viscosity, a=particle radius, v=relative approaching velocity of two particles and x=distance between particle surfaces. Physically, the lubrication of a contact can be viewed as a thin layer of viscous fluid that acts as a cushion between two particle surfaces. It slows down the initial particles velocities and decreases the kinetic energy of the particles. If the balance of the lubrication force and the fluid approaching velocities causes adjacent particles slowing down to near zero, the particles may stick next to each other and get trapped with the fluid and agglomerate.

The elastic rebound depends on the overlap of two particles if they are in contact with the real radii (r_{ij}<r_c) and the lubrication damping force acts upon contact when it is activated. The active particle radius is represented in DEM by the apparent radius that is bigger than the particle we want to model (Fig. 2).

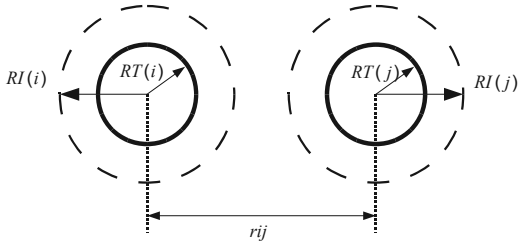

Figure 2. Schematic of the apparent (RI) and real (RT) radii and the approaching distance, r_{ij}.

The apparent radius enables the activation of the contact and calling the contact force when the particles approach each other at a close distance. During the time-stepping procedure, if the particles are close enough that they overlap with their real radii, then the elastic rebound and the friction are activated. The contact force logic can be written for PFC^{2D} for the user defined contact model, and compiled in C++ as:

if $r_{ij} \geq 2r_c = crit$ (10)

$$F_c = m\ddot{a} = -6\pi\mu a^2 \frac{v_{ij}}{x_{ij}} = -\mathrm{lub}\frac{v_{ij}}{(r_{ij} - 2r_c)}$$

if $r_{ij} < 2r_c = crit$ (11)

$$F_c = m\ddot{a} = k(2r_c - r_{ij}) + cv_{ij}$$

where F_c=contact force, d_{ij}=overlap of the particles, r_{ij}=distance between the particles centers, r_c=real particle radius, μ=fluid dynamic viscosity, k is the spring stiffness, c=dashpot constant, and lub=lubrication constant.

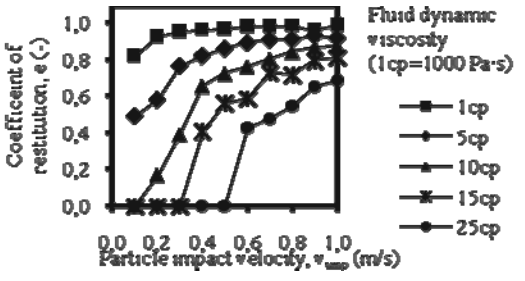

Figure 3. Particle drop test results for the sand particle with diameter d=0.25mm using user-defined lubrication force contact model

The coefficient of restitution of this system is non-linear curve dependent on the approaching velocity. Particle-particle interactions are governed by the user-defined contact model, and for the purpose of calculating their motion effect of fluid motion in fluid-solids coupled scheme they are averaged in each fluid cell (Eqn. 3). Fig. 3 shows the result of restitution coefficient simulation in PFC^{2D} using the developed user defined contact model for collision between sand particle and wall. Coefficient of restitution is the ratio between velocity after

and before impact. At low approaching velocities lubrication effect prevails and significantly decreases particle rebound velocity, while at higher impact velocities lubrication effect does not affect elastic rebound so much.

3 RESULTS

A study of 30 mesh sand flow in a narrow 2 mm and 4 mm wide and 0.5 m long channels reveals behavior of sand slurry flow obstructed with particle-particle interactions and particle-wall interactions caused by concentration and ratio of channel width and particle diameter. The study is simplified with respect to using a uniform particle size distribution and coarse discretization of the CFD-DEM fixed grid. Only two grid elements across the width of the narrow channel are able to be used in CFD scheme in order to keep the accuracy of the coupling with respect to the particle size. Boundary conditions of the flow are constricted to the non-slip conditions at the channel upper and lower boundary with zero fluid velocity, and a pressure difference ΔP between the enter and exit profiles of the channel. Average fluid and sand velocites are measured across some fixed volume in the channel after the flow was established. In a narrow channel, sand velocities are obstructed by formation of particle packs and solids-wall interactions.

Velocity of sand is always smaller than velocity of surrounding fluid, indicating that fluid flows arround the sand particles or packs that move with the fluid, but at slower velocity. Pressure and sand concentration effect on sand velocity in the narrow channel is studied. Fig. 4 shows the change of sand velocity under different presssure differences and sand concentrations. Average sand velocity in the channel decreases with particle concentration increase, but does not follow the same law for higher and lower (dp<500Pa) pressures. Fig. 5 shows the change of fluid velocity under different presssure differences and sand concentrations. Fluid velocity decreases with concentration increase, following similar paths for all pressure differences.

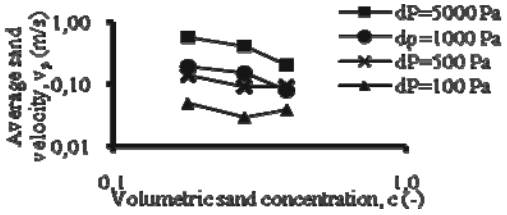

Figure 4. Sand velocity dependence on concentration at different pressures

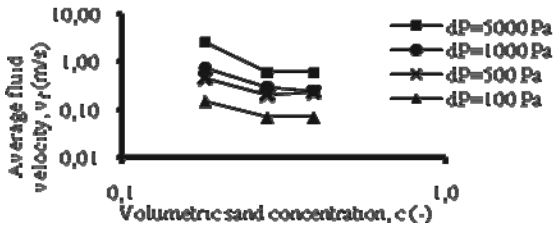

Figure 5. Sand velocity dependence on concentration at different pressures

Figs. 6 and 7 indicate that both sand and fluid follow the power-law dependence of velocity on sand concentration in log-log plot. The velocity slopes in log-log plot are parallel and increase with pressure decrease. However, if the sand velocity and fluid velocity ratio is observed, it seems that it generally rapidly decreases with pressure increase (Fig. 8) and then approaches steady value at very high pressures. This behavior can be related to stability of the flow and forming of particles clumps that force fluid to flow arround them. When fluid flows arround clumps, it flows in narrow channel and its velocity localy inceases because of that. Pressure increase enhances the frequency of particle collisions, whose damping causes agglomeration. Results shown in Fig. 8 indicate, as well, that velocities ratio depends on particles concentrations, not only on channel pressure. For higher initial particles concentrations (c_v=0.39) solids and fluid velocity ratio is more sensitive on pressure change than for lower initial concentrations (c_v=0.18).

Higher sand concentrations obstruct the increase of fluid phase flow velocity expected with pressure increase, as well as sand phase velocity increase, while lower concentrations have different impact on pressure dependent velocity. All the observed cases had velocities low enough for the flow to be considered laminar. (This can be seen in Figs. 6 and 7.)

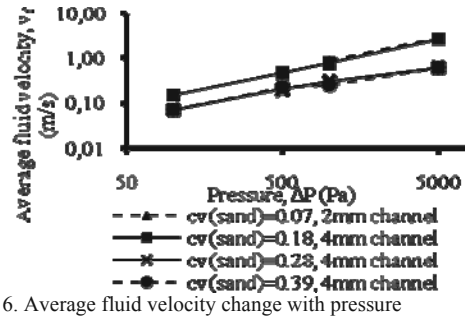

Figure 6. Average fluid velocity change with pressure

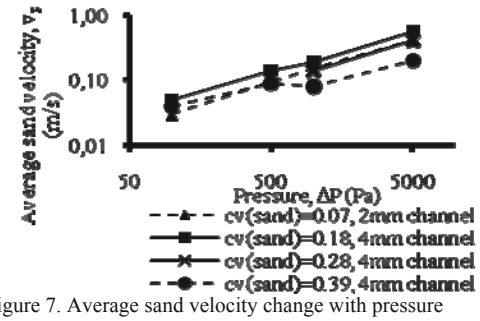

Figure 7. Average sand velocity change with pressure

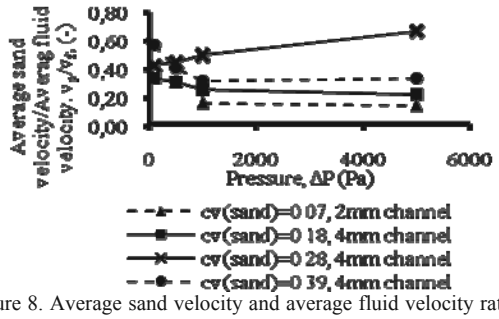

Figure 8. Average sand velocity and average fluid velocity ratio change with pressure

Attempts were made in the past to describe the sand slurry flow using the equivalent non-Newtonian parameters dependent on fluid and particle phase characteristics, such as fluid viscosity and sand volumetric concentration (Shah, 1993). The proposed formulation was based on the assumption that fluid and sand have the same velocities in the flow. However, here is shown that this assumption is not valid for the narrow channel and higher sand concentrations. The non-Newtonian parameters *K'* and *n'* that form apparent viscosity of the slurry (Eq. 8) at a given shear rate are investigated here with respect of fluid and sand phase separately. Non-Newtonian fluid low is:

$$\tau = K\dot{\gamma}^n = K\dot{\gamma}^{n-1}\dot{\gamma} = K\dot{\gamma}^{n'}\dot{\gamma} = \mu_a\dot{\gamma} \tag{8}$$

where τ=shear stress, $\dot{\gamma}$=shear rate, K=non-Newtonian fluid consistency index, n=non-Newtonian fluid flow-behavior index,

K'=slurry consistency index, *n'*=slurry flow behavior index and μ_a=slurry apparent viscosity.

The plots reveal some interesting trends. The non-Newtonian slurry index *K'* does not depend on sand concentration while the index *n'* is (Figs. 9 and 10). Index *n'* appears to decrease with increase of concentration, but at c_v=0.3 the trend changes and sand phase index rapidly increases. At this point the flow is characterized with pronounced formation of packs and clogs that affect the slurry flow into a channel.

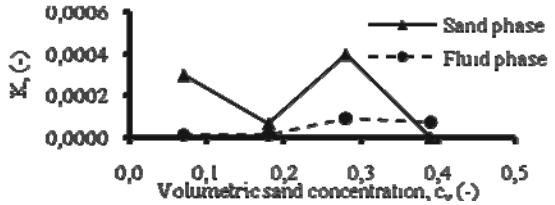

Figure 9. The *K'* fluid index for fluid and sand phase

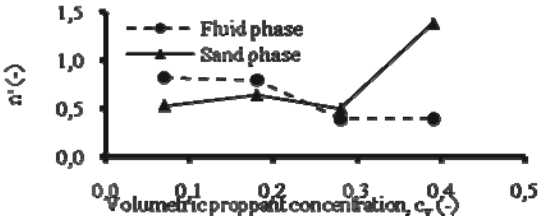

Figure 10. The *n'* fluid index for fluid and sand phase

At maximum sand concentration, the flow in the channel is completely stopped. Observation for both channel widths of 2mm and 4mm and pressures span 100-5000 Pa showed little dependence of clogging on the pressure difference in the channel. At higher pressures and higher concentrations, the initial velocities were larger for a while and then they decreased to a stabile level at which the flow continued. For the 2 mm wide channel (*D*/*W*=3.3, where *D*=channel width and *W*=particle diameter) the maximum volumetric sand concentration that was able to flow with a constant velocity was 0.14 while for the 4 mm wide channel it was 0.39. Attempts of model runs with higher concentrations showed a little bit of flowing but the flow stopped. Figs. 11, 12 and 13 show the clogged sand in a narrow fracture. At limiting value of sand concentration it can be seen that fluid flows arround the sand packs formed in the channel. This study uses numerical model to observe dense-phase fluid and solids flow in narrow channel, and more comprehensive laboratory study is recommended for future research.

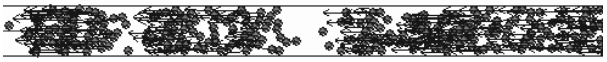

Figure 11. Clogging of sand in 4mm wide channel at initial volumetric sand concentration c_v = 0.49 with particles velocities vectors in direction opposite to the flow.

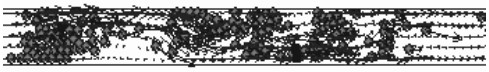

Figure 12. Unstable flow with formation of particles packs at initial c_v = 0.39 in 4mm wide channel with fluid flow velocity vectors around packs.

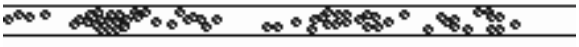

Figure 13. Formation of particles packs at initial c_v = 0.28 in 2mm wide channel.

4 CONCLUSIONS

A discrete element study of sand flow in narrow channels with higher concentrations up to the maximum concentration is studied. Maximum sand concentration is a value at which the sand transport is not possible and flow stops. The maximum sand concentration depends on channel width and particle diameter ratio, and it has a very low sensitivity to the magnitude of fluid pressure. At high pressures, slightly higher concentration than maximum was able to be transported only for a limited length along the channel. Velocity of the sand and fluid velocity have different magnitudes, and the sand is being transported in a slurry at velocities lower than the fluid. At higher concentrations, sand forms packs and clogs, and fluid flows around them. Since the two phases, solid phase and fluid phase, do not have same average velocities, and it is not possible to simply describe slurry as a mixture of two phases with and substitute equivalent power-low (non-Newtonian) fluid parameters. Both fluid and sand average velocities increase proportionally with the pressure increase. However, if the sand velocity and fluid velocity ratio is observed, it seems the generally decrease with pressure increase. In other words, using higher fluid pressures less difference in sand and fluid flow velocity can be expected. Power-law behavior of phases can be captured to describe the flow, but since the two phases have different average velocites it is hard to average and come up with unique slurry flow characterization at this point. A more comprehensive study is needed to address this issue.

5 ACKNOWLEDGEMENTS

Financial support provided by the U.S. Department of Energy under DOE Grant No. DE-FE0002760 is gratefully acknowledged. The opinions expressed in this paper are those of the authors and not the DOE.

6 REFERENCES

Bouillard, J., R. Lyczkowski, and D. Gidaspow, 1989, Porosity distributions in a fluidized bed with an immersed obstacle: AIChE Journal, v. 35, p. 908-922.

Crowe, C. T., J. D. Schwarzkopf, M. Sommerfeld, and Y. Tsuji, 2011, Multiphase flows with droplets and particles, CRC press.

Cundall, P. A., and O. Strack, 1979, A discrete numerical model for granular assemblies: Geotechnique, v. 29, p. 47-65.

Davis, R. H., J. M. Serayssol, and E. Hinch, 1986, The elastohydrodynamic collision of two spheres: Journal of Fluid Mechanics, v. 163, p. 479-497.

Patankar, S. V., 1980, Numerical heat transfer and fluid flow, Hemisphere Pub.

Shah, S., 1993, Rheological characterization of hydraulic fracturing slurries: Old Production & Facilities, v. 8, p. 123-130.